THE JOURNAL OF PHYSICAL CHEMISTRY A
A JOURNAL OF THE AMERICAN CHEMICAL SOCIETY

pubs.acs.org/JPCA

Article

Low-Energy Electron Inelastic Mean Free Path of Copper

Daniel Sier,* Jay D. Bourke,* and Christopher T. Chantler*

Cite This: J. Phys. Chem. A 2026, 130, 1940−1947

Read Online

ACCESS | Metrics & More | Article Recommendations

ABSTRACT: A new method is presented for the measurement of electron inelastic mean free path (IMFP) of copper metal from the K-edge X-ray absorption fine structure (XAFS) using energies from 5 to 320 eV above the edge. The accuracy of theoretical determinations of electron IMFP at low energies is one of the key limiting factors in current XAFS modeling and Monte Carlo transport. Significant discrepancies between theoretical and experimental IMFP values have been revealed through recent studies, posing significant questions regarding the accuracy of key structural parameters extracted through XAFS analysis. Small molecules and organometallic systems, which often lack robust tabulations of key electron scattering data, are particularly susceptible to inconsistencies in the IMFP, requiring a new methodology to resolve these discrepancies. XAFS is determined using an advanced density functional theory (DFT) core of the finite difference method for XAFS (FDMX). The popular multiple-scattering approach, based on muffin-tin potentials, is shown to be inadequate for accurately calculating the fine structure. Experimental IMFP measurements are both consistent with past measurements and consistent with the latest plasmon theory. However, variation of measurements with temperature points to the need for fine spacing at room temperature and measured uncertainties of data points at low temperatures and also suggests significant temperature-dependent effects both of broadening and correlation from multiple sources. This work confirms both recent past experimental and theoretical works and points to new areas of challenge and discrepancy.

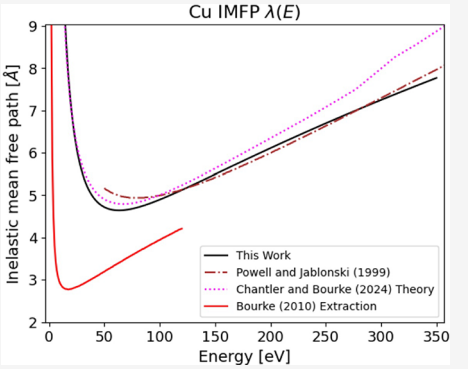

INTRODUCTION

Electron Inelastic Mean Free Path (IMFP)

The electron inelastic mean free path (IMFP) is one of the most fundamental parameters in materials science. It represents the average distance between inelastic collisions of an electron traveling through a medium with a given energy. This makes it extremely useful for a range of microscopic techniques that rely on electrons as the probe. These include X-ray photoelectron and Auger-electron spectroscopy (XPS, AES),[1] electron energy loss spectroscopy (EELS),[2] and low-energy electron diffraction (LEED).[3] Uncertainty in the electron IMFP in almost all solid-state systems at energies below 50 eV presents key limitations to the accuracy of current XAFS modeling and Monte Carlo transport simulations.

While the understanding of inelastic scattering remembers Drude, Einstein, Debye, and Sommerfeld from 1900 through 1928, it is perhaps surprising that extensions of these bases remain active and prevalent in 2025. Major advances of free-electron gas (FEG) models were made[4,5] over the intervening decades. Observations of plasmons via the energy losses in units of $\hbar\omega_p$ experienced by electrons when passing through thin metallic films[6] led to the development of plasma oscillation and propagation theories. A major breakthrough in the understanding and modeling of electron properties came with Penn in 1987,[7] which was then able to link up arbitrary solid-state structure and behavior from experimental or theoretical optical-limit data to evaluate electron and plasmon inelastic scattering from band theory. Recent observations of discrepancies in IMFP theory at energies below 200 eV[8−10] have provided further insight and led to new developments of coupled plasmon theory.[11,12]

The IMFP is typically expressed in terms of the optical dielectric function $\epsilon(q, \omega)$:[13]

$$\lambda^{-1}(E) = \frac{\hbar}{a_0 \pi E} \int_0^{E-E_F/\hbar} \int_{q_-}^{q_+} \frac{1}{q} \mathrm{Im}\left[\frac{-1}{\epsilon(q, \omega)}\right] dq d\omega \quad (1)$$

where $q_\pm = \sqrt{\frac{2mE}{\hbar^2}} \pm \sqrt{\frac{2m}{\hbar^2}(E - \hbar\omega)}$, and $\mathrm{Im}\left[\frac{-1}{\epsilon(q,\omega)}\right]$ is often referred to as the energy loss function (ELF).

However, the ELF, and by extension the IMFP, has proven difficult to determine for low electron energies,[14] with existing databases showing significant variation below 100−200 eV.[15]

Received: January 12, 2026
Revised: February 9, 2026
Accepted: February 10, 2026
Published: February 20, 2026

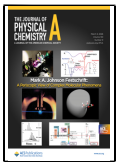

https://doi.org/10.1021/acs.jpca.6c00232
J. Phys. Chem. A 2026, 130, 1940−1947

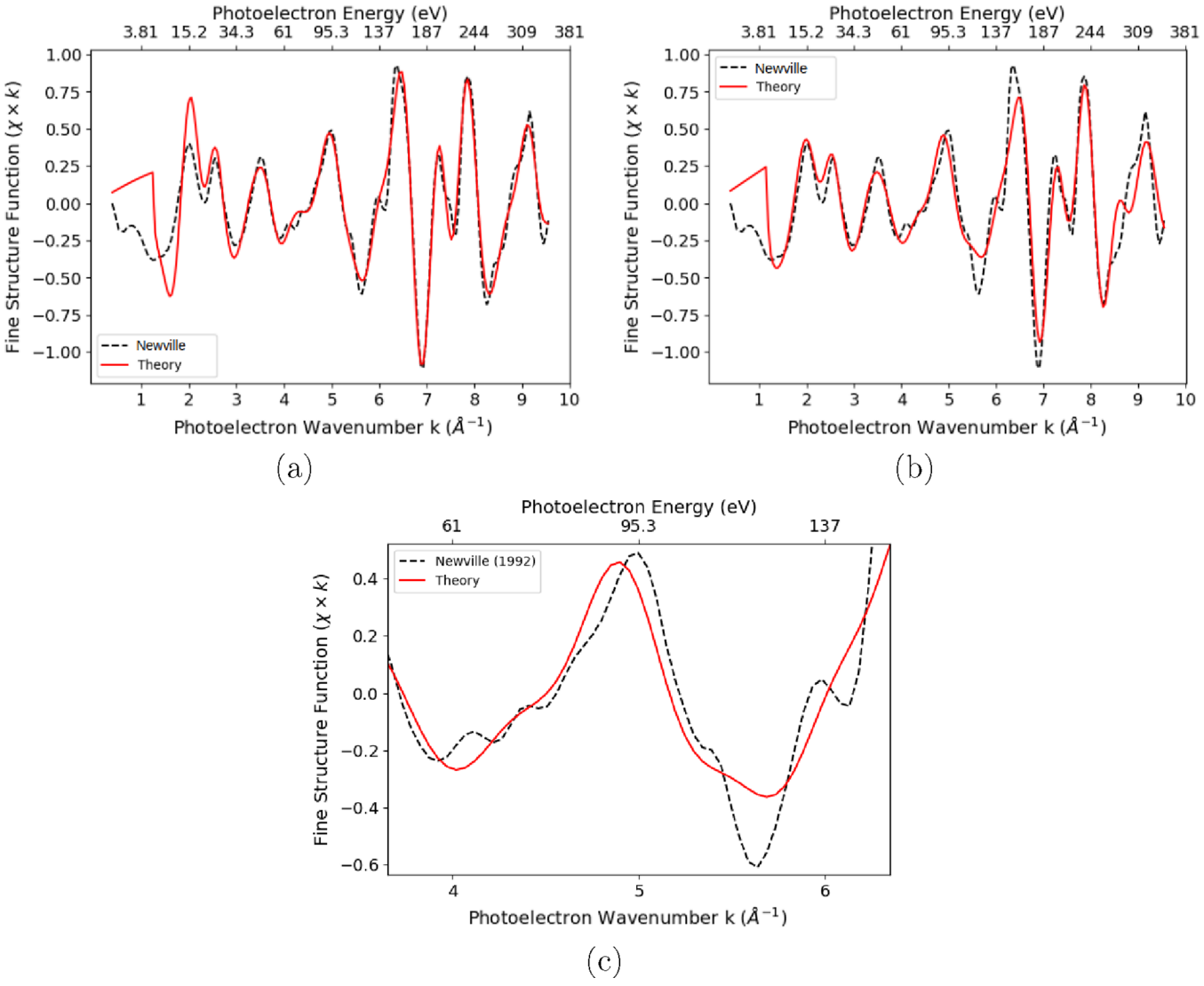

Figure 1. Cu K-edge XAFS spectra of metallic copper at 10 K[25,26] fitted using FEFF 8.1 (a) with a k-range of $3.5 < k < 10.0$ and (b) $1.1 < k < 10.0$. 37 paths were modeled, covering scattering path lengths shorter than 7 Å. Path lengths and σ^2_{DW} were freely fitted for each of the first three nearest-neighbor scattering paths. All other path lengths were assigned a common scaling factor and a common σ^2_{DW}. The wide fitting k-range has discrepancies throughout the range. Even the narrow k-range $3.5 < k < 10.0$ has several missing peaks and structures. (c) Looking closely at some sections of $3.5 < k < 10.0$ comparison reveals that significant structures remain unexplained by FEFF, even with free fits.

Most theoretical predictions have significant limitations in approximations and are usually unable to compute electron−phonon scattering[16] or electron−plasmon interactions.[12] Experimental measurements of the IMFP, usually conducted using elastic peak electron spectroscopy (EPES),[17] also struggle at low energies due to the emergence of secondary-electron effects and uncertainties in elastic-scattering cross sections, with results not considered accurate below 50 eV. These experimental techniques also usually struggle to isolate elastic damping from inelastic damping, as the processes are usually indistinguishable and hence inseparable. This energy region is of great importance to XAFS, and more specifically XANES analysis, where the IMFP has significant influence upon the backscattered photoelectron wave function. Common databases for visible-frequency (i.e., the zero-frequency limit $\epsilon(q, \omega = 0)$) optical properties include Hagemann et al.[18] and Palik,[19] which are often used as reference benchmarks for the zero-energy transfer energy dielectric constant prior to extension into q-space.[20,21]

All of these issues call for accurate data on the IMFP of elemental and compound structures down to low energy. We achieve this herein by extracting the IMFP from high-accuracy K-edge XAFS measurements of copper. XAFS is highly dependent upon the IMFP as the XAFS signal results from the backscattering of the excited photoelectron traveling through the material and can be expressed in the standard EXAFS equation:

$$\chi(k) = \sum_i \frac{N f_i(k)}{kR_i^2} e^{-2k^2\sigma_i^2} e^{-2R_i/\lambda} \sin(2kR_i + \delta_i(k)) \quad (2)$$

In particular, and unlike other possible experimental techniques, the elastic interaction strengthens the XAFS oscillation, while the inelastic interaction dampens the oscillation, so that the two competing processes can be orthogonalized. While there are several effects that contribute to the modulation and damping of the XAFS signal, the IMFP is most significant in the region up to

https://doi.org/10.1021/acs.jpca.6c00232
J. Phys. Chem. A 2026, 130, 1940−1947

a photoelectron energy $E_e \approx 250-350$ eV. Hence, accurate XAFS data is ideal for measuring IMFPs at low energies.

Limitations of FEFF

Perhaps the most popular EXAFS theoretical code is FEFF,[22−24] which uses a spherically corrected plane wave and muffin-tin potentials to model the scattering and self-interference of the photoelectron and thus determine the XAFS and is capable of producing accurate spectra in the EXAFS region. However, this approach makes several assumptions about the behavior of the photoelectron, causing the theory to break down at low energies. When the theory is used to fit experimental data, discrepancies remain.

To illustrate this, we introduce key reference works on the experimental XAFS spectrum of copper above the K-edge: Newville from his Ph.D. thesis in 1995, at 10 K;[25,26] Tran following his Ph.D. thesis;[27,28] Glover;[29] and Newville and Ravel at room temperature from the International Tables for Crystallography.[30]

Figure 1 presents the experimental Cu K-edge XAFS spectrum of metallic copper fitted over two separate k-ranges of (a) $3.5 < k < 10.0$ and (b) $1.1 < k < 10.0$ using FEFF 8.1. Figure 1a suggests that FEFF performs fairly well at high k values when excluding low k regions from the fit, but there is a significant discrepancy close to the edge. Figure 1b demonstrates that when these low k regions are included, the agreement is poor across the range of k fitted. Furthermore, even for the narrow-range fit (Figure 1c), there are regions where FEFF fails to predict peaks and the structure of the XAFS.

Since the electron IMFP signatures are observed at low energies, where the photoelectron kinetic energies are below 350−500 eV and where XAFS is most sensitive to the IMFP, we require an alternate theory for XAFS to measure and extract the IMFP. We use the Finite Difference Method for XAFS (FDMX) software package[31] following the finite difference method for near edge structure (FDMNES),[32,33] using density functional theory (DFT) and TD-DFT.

METHODS

Calculations

To ensure accurate results, our theoretical spectra presented here followed our guidelines for the interpoint grid spacing on which the FDM calculations are performed, as outlined in our FDMX[31] manual:

$$d = \begin{cases} 0.24\ \text{Å}, & E \le 100 \\ 0.20\ \text{Å}, & 100 < E \le 200 \\ 0.16\ \text{Å}, & 200 < E \le 350 \\ 0.14\ \text{Å}, & 350 < E < 700 \end{cases} \tag{3}$$

Due to this increasing density of grid points, the calculation radius was decreased with energy, as follows:

$$R = \begin{cases} 14.0\ \text{Å}, & E \le 100 \\ 10.0\ \text{Å}, & 100 < E \le 200 \\ 8.5\ \text{Å}, & 200 < E \le 350 \\ 7.0\ \text{Å}, & 350 < E < 700 \end{cases} \tag{4}$$

Furthermore, the keyword "`lmaxfree`" was used to remove the restriction on expansions in the spherical harmonics with higher energies, ensuring more accurate calculations in this region.

Fitting Procedure

To fit the fine structure in Figure 1, both the experimental data $\left[\frac{\mu}{\rho}\right]_{\text{exp}}(E)$ and FDMX calculations $\left[\frac{\mu}{\rho}\right]_{\text{th}}(E)$ must have their background absorption $\left[\frac{\mu}{\rho}\right]_0$ removed. As the experimental data was collected in transmission mode, this is achieved by first fitting and subtracting a function for the pre-edge region of the data, below the K-edge $\left[\frac{\mu}{\rho}\right]_{\text{p}}$:

$$\left[\frac{\mu}{\rho}\right]_{\text{p}} = AE^{\text{B}} \tag{5}$$

where E is the X-ray photon energy and A and B are fitting parameters. Next, our Mu2Chi background subtraction package[34] was used to solve for $\left[\frac{\mu}{\rho}\right]_0$ by fitting a spline to the data to extract χ.

To isolate χ from the FDMX output, $\left[\frac{\mu}{\rho}\right]_0$ was calculated by specifying a very small value for the radius in the input file. This value should be significantly smaller than the nearest-neighbor separation and typically less than 1 Å, below which there is no change in the output. Interpoint distances follow eq 3.

Once the fine-structure spectra have been obtained, a number of corrections must be applied in order to achieve agreement with the experimental measurements. The first of these is the broadening due to the lifetime of core-hole state, which introduces some intrinsic uncertainty into the energy of photoelectron. The resulting photoelectron will have an energy distribution characterized by a Lorentzian:

$$L(E, \Gamma) = \frac{1}{\pi}\left[\frac{\Gamma_{1s}}{E^2 + \Gamma_{1s}^2}\right] \tag{6}$$

where Γ_{1s} is the energy lifetime width of the 1s hole and represents the half-width at half-maximum (HWHM) of the distribution. Thus, to correct for the core-hole lifetime, the raw FDMX spectra must be convolved by a Lorentzian of the appropriate width:

$$\chi(E) = (\chi_0 \times L)(E) \tag{7}$$

where χ_0 is the fine structure function for a system without core-hole lifetime uncertainty.

The IMFP will also introduce an energy uncertainty similar to that of the photoelectron. This can be thought of like core-hole broadening, where a finite IMFP implies a state only has a certain lifetime associated with it, resulting in a similar Lorentzian energy broadening, the width of which is

$$\Delta E_{\text{IMFP}} = \frac{\hbar}{2\lambda(E)}\sqrt{\frac{2E}{m_e}} = \Gamma_\lambda(E) \tag{8}$$

Thus, similarly to the lifetime hole width, the IMFP introduces additional Lorentzian broadening to the absorption spectrum. This formalism can also be derived using the self-energy treatment,[35,36] where $\Gamma_\lambda(E)$ is replaced with $\Sigma(E)$, and we treat the effective spectral function $A_{\text{eff}}(\omega, \omega')$ as a Lorentzian.

The final correction is due to the effects of thermal motion of the atoms, where slight deviations from equilibrium positions will cause each photoelectron to effectively 'see' a slightly different lattice. This is accounted for as in multiple-scattering analysis by multiplying an exponential dampening factor:[37]

$$\chi(k) = \chi_0(k)e^{-\sigma^2k^2/2} \tag{9}$$

Modeling the IMFP

Theoretically calculating the electron IMFP involves evaluating the ELF. A number of empirical models have been created that attempt to model the evolution of the IMFP with energy. These include the Tanuma−Powell−Penn Formula,[13] a modified form of the Bethe equation:

https://doi.org/10.1021/acs.jpca.6c00232
J. Phys. Chem. A 2026, 130, 1940−1947

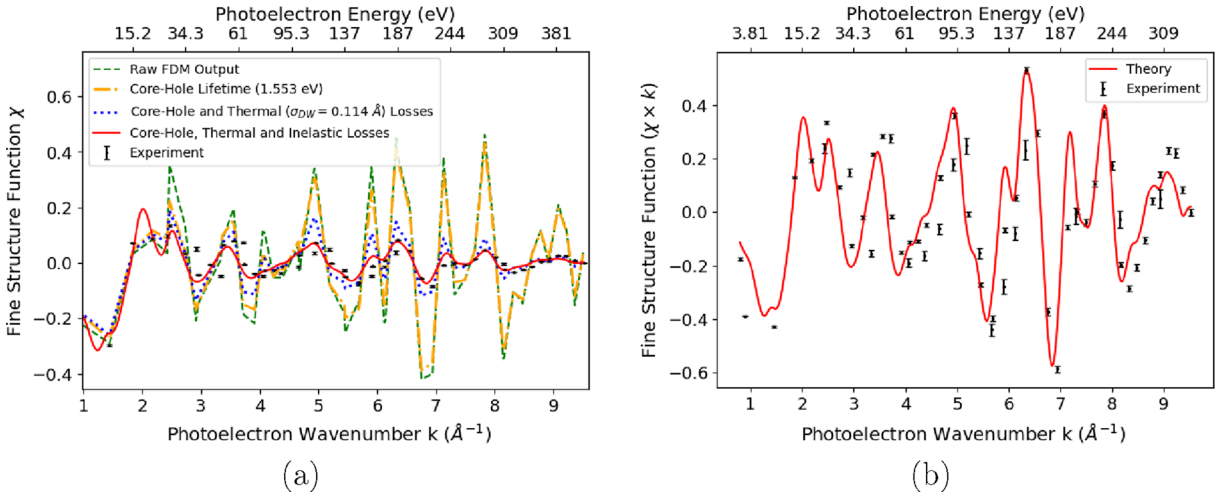

Figure 2. XAFS spectrum above the copper K-edge. (a) Impact of each contribution to the broadening of the theoretical spectrum. (b) Final result, scaled by *k*, highlighting oscillations at higher energies.

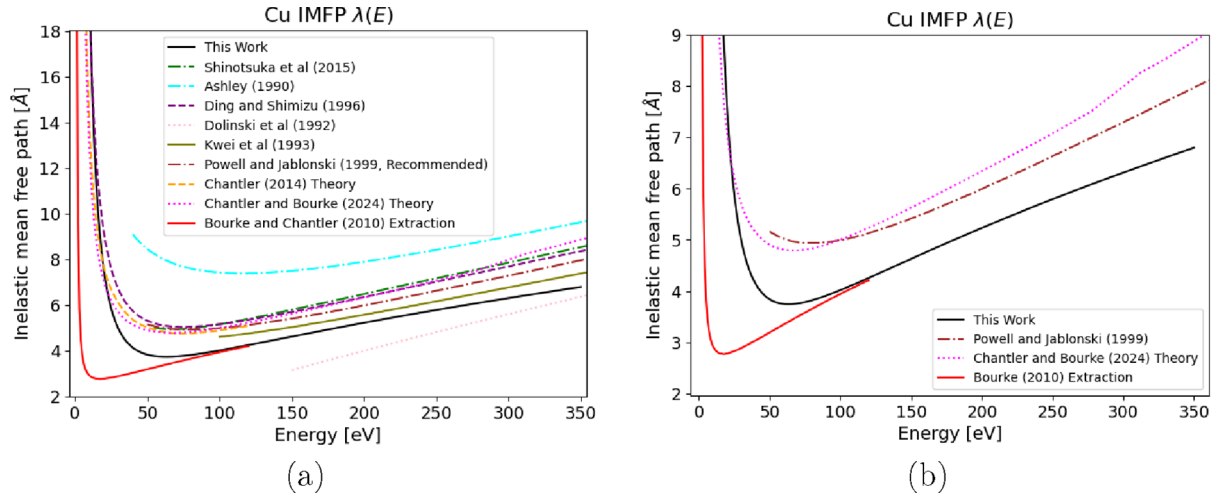

Figure 3. (a) Extracted IMFPs for the copper fit in Figure 2, compared with the literature. Results of Shinotsuka et al.[55] and Powell and Jablonski[51] are obtained by determining the dependence of the inelastic scattering probability on energy loss through use of the Penn algorithm[7] to relate the Lindhard dielectric function $(\epsilon(q, \omega))$[56] to experimental optical data $(\epsilon(q, 0))$. Ashley[49] used a similar method but included exchange effects. Ding and Shimizu[52] utilized Monte Carlo simulations of electron-scattering processes and the energy of secondary electrons. Kwei et al.[48] used an extended Drude dielectric function to incorporate plasmon excitations and interband transitions. Experimental measurements of Dolinski et al.[54] compared EPES measurements with Monte Carlo simulations of the elastic backscattering probability to determine the IMFP. Recent theory from Chantler and Bourke[50] and Bourke[53] defines a new Lindhard partial-pole model to explicitly consider plasmon broadening on the electron, ensuring that the obtained optical ELF matches that determined via density functional theory (WIEN2K). (b) Comparisons of our results with previous measurements of Bourke and Chantler,[9] the most commonly cited semiempirical modeling of Powell and Jablonski,[51] and the latest theory[53] are presented for clarity.

$$\lambda = \frac{E}{E_p^2(\beta \ln \gamma E - C/E + [D/E]^2)} \tag{10}$$

where $\beta = -0.1 - \frac{0.944}{\sqrt{E_p^2 + E_g^2}} + 0.69\rho^{0.1}$, $\gamma = 0.191\rho^{-0.5}$, $C = 1.97 - 0.91U$, $D = 53.4 - 20.8U$, and $U = \frac{1}{829.0}E_p^2$, ρ is the density (g/cm^3), E_g is the band gap energy (for semiconductors), and E_p is the bulk plasma energy in eV. Another formula is that of Gries:[38]

$$\lambda = \frac{k_1 V_a}{Z^*} \frac{E}{\log_{10}(E) - k_2} \tag{11}$$

where V_a is the atomic volume in units of cm^3/mol, Z^* is the number of effective interaction-prone electrons per atom, k_1 and k_2 are fitted parameters. However, both of these formulas and functional forms are only designed to operate in high-energy regions (>50 eV), with singularities often appearing at low energies.

One approach that avoids this problem is the so-called 'universal curve' of Seah and Dench.[39] The high-energy $(\sqrt{E})$ behavior seeks to mimic that of eq 10. The low-energy behavior is based on that put forward by Quinn[40] and Sze et al.,[41] which state that the scattering probability should be proportional to the product of accessible filled and unoccupied electron states, giving:

$$\lambda = \frac{A}{E^2} + B\sqrt{E} \tag{12}$$

where *A* and *B* are fitted parameters. However, as discussed in Jablonski and Powell,[42] and in Powell and Jablonski,[43] the data that was used to derive this relation was obtained using low-energy electron diffraction via the overlay technique.[44] Thus, this equation corresponds to the effective attenuation length (EAL), which also includes elastic-scattering processes rather than the true IMFP. At lower energies (<100 eV), elastic-scattering processes are strong relative to inelastic scattering, making this approach unsuitable for our needs.

https://doi.org/10.1021/acs.jpca.6c00232
J. Phys. Chem. A 2026, 130, 1940−1947

The final methodology we consider is that used by Chantler and Bourke,[8] where the convolution width $\Gamma(E)_{\mathrm{IMFP}}$, as defined in eq 8, is modeled with the following functional:

$$\Gamma_{\lambda}(E) = \frac{\sum_{i=1}^{n} E^{i \cdot x_0}}{\sum_{i=1}^{n} \frac{1}{x_i} E^{i \cdot x_0}} \tag{13}$$

where x_i are the n fitting parameters. This form shares similarities with eq 12, as in the high-energy limit, the convolution width reduces to a constant (specifically x_n), meaning that through eq 8 $\lambda \propto \sqrt{E}$. At lower energies, however, it is far more flexible, enabling more complex behavior in the transition from the low- to high-energy region. It is this final method of Chantler and Bourke[8] that we used to model the IMFP in our fitting procedure.

RESULTS AND DISCUSSION

Development of IMFP Measurement

This work builds on Bourke and Chantler.[9,8] The current work uses a significantly improved fitting function, which performs the complex convolutions via fast Fourier transforms (FFTs) to perform equivalent fits roughly 2 orders of magnitude faster. While the new convolution code has been demonstrated to perform comparably to the previous methodology, we test the new code and general methodology to confirm that they are capable of obtaining results consistent with the literature.

We perform an analysis of the same K-absorption edge of copper as in Bourke and Chantler.[9] The experimental data for these comparisons follow Glover et al.[29] and Chantler et al.[28]

The crystal structure of copper is an fcc lattice ($Fm\bar{3}m$ space group), consisting of a four-atom basis positioned at (0, 0, 0), $\left(0, \frac{1}{2}, \frac{1}{2}\right)$, $\left(\frac{1}{2}, 0, \frac{1}{2}\right)$, and $\left(\frac{1}{2}, \frac{1}{2}, 0\right)$ in the unit cell, with edge lengths $a = b = c = 3.6149$ Å and internal angles $\alpha = \beta = \gamma = 90°$. The room-temperature structure used to generate the FEFF structure for this investigation follows:[45]

$$\alpha_{\mathrm{T}} = \alpha_0 e^{CE_{\mathrm{T}}}; E_{\mathrm{T}} = \int_0^T C_{\mathrm{V}}(T) dT \tag{14}$$

where α_T and α_0 are the lattice constants at temperature T and at absolute zero, respectively, C and C_V are the specific heat capacity and specific heat capacity under constant volume, respectively.[46] The room-temperature structure used for this investigation follows,[47] with a lattice spacing of 3.61496 Å. For 10 K, the lattice spacing was estimated to be 3.605 Å with the above formulas.

Figure 2 presents theoretical spectra generated and fitted to the data. The fine structure was isolated from the experimental data using *mu2chi*, with a 15-knot spline being found to give the lowest χ_r^2 when fitting the FDMX spectra. A fitting range from 11 to 320 eV ($1.7 < k < 9.2$ Å^{-1}) above the Fermi level was found to have a suitable lowest energy bound. For a lower minimum k for the fitting range, the fit became unstable.

Figure 3 compares the extracted IMFP with a variety of sources, including theoretical calculations of Kwei et al.,[48] Tanuma et al.,[13] Ashley,[49] Chantler and Bourke,[50] Powell and Jablonski,[51] Ding and Shimizu,[52] and Chantler and Bourke,[53] as well as experimental measurements of Dolinski et al.[54] and Bourke and Chantler.[9]

Here, we see excellent agreement with previous measurements at higher energies. However, at lower energies, discrepancies begin to emerge, with the fitted values being slightly lower than predicted. The most likely explanation for the differences in extracted IMFPs between this work and that of Bourke and Chantler[9] is due to the different methods of fitting the background absorption, which primarily impacts very low photoelectron energies. Bourke and Chantler[9] fitted the FDMNES background plus a decaying exponential to the data, as opposed to our spline fitting. Bourke and Chantler[9] only differ significantly from the current result at lower energies close to the edge, which explains why the two sets of extracted IMFPs converge at higher energies. Comparisons with theories[50,53] show consistently lower values of the IMFP than those extracted.

Table 1 presents the fitted parameters. The extracted 1*s* hole-width (Γ_{1s}) of 1.55 eV is identical to 1.55 eV from Krause and Oliver.[57] Large correlations between the hole-width and the IMFP at low energies introduce large uncertainty into our extracted value, though the formal uncertainty will be a significant overestimate if the other IMFP parameters (x_0, x_1, and x_2) are defined well. The extracted hole-width also compares very well to the updated value of 1.49 eV recommended by Campbell and Papp.[58]

Table 1. Fitted Parameters for the IMFP above the Cu Absorption Edge for Room Temperature XAFS[a]

parameter	value	σ_{sd}
x_0	2.16	0.34
x_1	4.8×10^{-3}	7.2×10^{-3}
x_2	10.8	1.3
σ_{DW} (Å)	11.39×10^{-2}	0.19×10^{-2}
E_{edge} (eV)	8980.04	0.073
Γ_{1s} (eV, FHWM)	1.55	1.1
χ_r^2	155	

[a] x_{0-2} correspond to the parameters in eq 13 for $\lambda(E)$

Fitted values of the Debye–Waller factor for copper ($\sigma_{DW,fit}$ = 0.1139 Å) compare well with theoretical values determined using the methods first described by Beni and Platzman[59] and later corrected by Greegor,[60] which give the mean-square displacements of neighboring atoms relative to an unmoving central atom as $\sigma_{DW,theory}$ = 0.1354 Å.

Excellent agreement of better than 1 eV also results from comparison of extracted values of the copper K-edge energy, 8980.04 eV, compared with 8979 eV from the historical research of Bearden[61] and 8980.48(2) eV from the more recent and more reliable research by Kraft et al.[62] In other words, the extraction of the IMFP appears not to distort the other parameters, and the result appears very consistent with literature expectations, helping to justify the values and uncertainties of the IMFP functional used. Changing the functional form will naturally affect the shape and fit of these other parameters, as well as the resulting IMFP. This new test of the old and new extraction of IMFP yields compelling results.

First IMFP Measurement at Low Temperature

The data discussed above is highly accurate, which increases the χ_r^2 compared with standard measurements. However, the data is sparse compared with numerous typical XAFS data sets, so we look to another alternate view, to make an additional test, with small point spacing and sharper structure, namely using a copper data set collected at 10 K. We therefore use measurements taken at the National Synchrotron Light Source (NSLS) on the X11A beamline, of a copper foil at 10K in transmission mode.[25,26] This data was accessed from the International X-ray Absorption Society's (IXAS) X-ray Absorption Data Library. The measurements have no quantification of any uncertainties and no error

https://doi.org/10.1021/acs.jpca.6c00232
J. Phys. Chem. A 2026, 130, 1940−1947

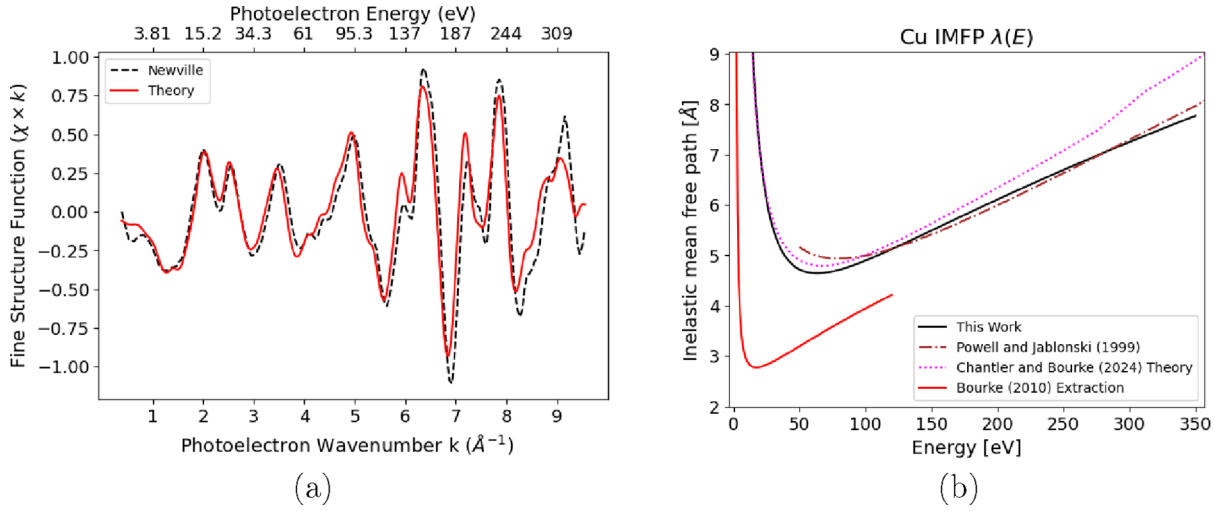

Figure 4. (a) Fit of the K-edge XAFS of copper at 10K.[25,26] (b) Corresponding extracted IMFP compared with previous measurements and theory. The extracted IMFP increases compared to the extraction from the previous data sets in Figure 3. The point spacing is much finer, the structure is sharper at the low 10 K temperature, yet the absence of uncertainty propagation means that χ^2_r does not have a well-defined meaning.

field for the data points, yet the very small step size makes it suited to this alternate analysis. Furthermore, the low temperature at which the measurements were conducted results in a significant reduction in thermal broadening, in principle, allowing for a more accurate IMFP extraction.

After the removal of pre-edge structure using eq 5, an 11 knot spline was found to give the lowest χ^2_r when fitted to the data to isolate the fine structure. This data was fitted over 1.15 Å^{-1} < k < 9.16 Å^{-1}, i.e. from 5 to 320 eV above the Fermi level, so for photoelectron energies from 5 to 320 eV.

Figure 4 shows remarkable agreement between XAFS theory and experiment, and an IMFP that is in excellent agreement with theory.[50,53] At low energies (<50 eV), the extracted IMFP and the most recent predictions of Chantler and Bourke[53] are in almost perfect agreement. At higher energies, the results appear closer to those of Chantler and Bourke[50] and Powell and Jablonski[51] rather than to those of Chantler and Bourke.[53] Formal theory for IMFP and thermal behavior are best defined at the lowest temperature, and they are expected to vary with temperature. Perhaps this is a first sign of such behavior.

Table 2 presents the fitted parameters. Because there were no input data uncertainties, we provide no fitting uncertainties, and

Table 2. Extracted Parameters from Fitting the Low Temperature (10 K) Dataset[26]

parameter	Cu
x_0	1.63
x_1	0.0261
x_2	9.67
σ_{DW} (Å)	8.74×10^{-2}
E_{edge} (eV)	8976.5
Γ_{1s} (eV, FHWM)	1.48

χ^2_r is not meaningful. The excellent agreement of the extracted IMFP from the low-temperature copper data indicates that, even at low energies, static or thermal disorder contributed significantly to the broadening of XAFS spectra. These results suggest some 25% reduction of static and thermal isotropic broadening at low temperature compared with room temperature, which is plausible.

The resulting edge energy is suspiciously low (8976.5 eV rather than 8980.48(2) eV from Kraft et al.[62]). This could be due to energy calibration errors in the data set or to correlation in fitting errors and uncertainties. The hole width, in conventional relativistic quantum mechanics, might be expected to be a constant with temperature; but the overall broadening is certainly reduced at low temperature, and 1.48 eV is broadly consistent, probably within uncertainty, with the room-temperature results of 1.55 eV, and certainly consistent with Campbell and Papp.[58]

The challenges at low k and low photoelectron energy for the room-temperature extraction are broadly consistent with a recent attempt to explain the discrepancy in the room-temperature-extracted IMFP by Ridzel et al.[15] based on Brown et al.,[16] who found that taking into account the electron−phonon IMFP was important for achieving agreement between theoretical calculations and the results of Bourke and Chantler[9] down to 20 eV.

CONCLUSIONS

We have presented measurements of the electron inelastic mean free path for copper from 2 to 350 eV. Excellent agreement between experiment and theory for the XANES and XAFS are obtained, both from room temperature measurement and separately from low temperature measurement at 10 K.

Measurement of IMFP was achieved through the development of an entirely new fitting procedure that is several orders of magnitude more efficient than previous work. We also compare existing theories for predicting IMFP at low energy. We show that it is possible to measure the IMFP across the entire XAFS region, including both XANES and EXAFS, with high accuracy.

The extracted IMFP from room-temperature measurements is smaller than that predicted by theory,[50,53] in agreement with past room-temperature experiment.[9] This apparently lower experimental IMFP at low photoelectron energies could be due to thermal effects, correlated uncertainties, and variation of IMFP and σ_{DW} with temperature.

Fits of theory to low-temperature (10 K) XAFS measurements reveal an IMFP that is in excellent agreement with established and recent coupled plasmon theory, noting the absence of defined data uncertainties.

https://doi.org/10.1021/acs.jpca.6c00232
J. Phys. Chem. A 2026, 130, 1940−1947

The need for an improved understanding of the nature of the effect of thermal oscillations on the XAFS is also illustrated, with conventional dampening methods producing poorer agreement with experiment than when modeling the effect as a convolution. The results obtained indicate that XAFS and IMFP may be highly dependent on temperature even at low energies. Further low-temperature measurements will be invaluable.

In summary, until further experimental measurements are conducted with well-defined uncertainties, both data sets and the results appear well-defined and valid. The room-temperature extraction of IMFP may, and indeed will, be affected by all thermal broadening of both the thermal ellipsoid σ_{DW} and thermal broadening of the inelastic mean free path IMFP. The room temperature extraction of IMFP is also correlated with uncertainties of E_{edge} and with the hole width Γ_{1s}. Any of these details may explain possible impacts of temperature, certainly at higher k and higher photoelectron energies, and the extraction certainly assumed that measurements below ≈ 120 eV might not be significantly affected by thermal motion. Our results here suggest that thermal effects and static disorder may be significant at 10 K and may impact the extracted IMFPs.

AUTHOR INFORMATION

Corresponding Authors

Daniel Sier − *L'Orme des Merisiers, Synchrotron SOLEIL, Saint-Aubin 91190, France*; Email: daniel.sier@synchrotron-soleil.fr

Jay D. Bourke − *School of Physics, University of Melbourne, Parkville, Victoria 3010, Australia*; Email: jaydbourke@gmail.com

Christopher T. Chantler − *School of Physics, University of Melbourne, Parkville, Victoria 3010, Australia*; orcid.org/0000-0001-6608-0048; Email: chantler@unimelb.edu.au

Complete contact information is available at: https://pubs.acs.org/10.1021/acs.jpca.6c00232

Notes

The authors declare no competing financial interest.

ACKNOWLEDGMENTS

The authors acknowledge contributions to the fitting code by Ethan Koren, the University of Melbourne Research Computing Services and the Petascale Campus Initiative. They acknowledge the financial support provided by the Australian Research Council (ARC), Grant ID: DP210100795.

REFERENCES

(1) Powell, C. J.; Jablonski, A.; Tilinin, I.; Tanuma, S.; Penn, D. R. Surface sensitivity of Auger-electron spectroscopy and X-ray photoelectron spectroscopy. *J. Electron Spectrosc. Relat. Phenom.* **1999**, *98*, 1−15.

(2) Fuentes, G.; Elizalde, E.; Yubero, F.; Sanz, J. Electron inelastic mean free path for Ti, TiC, TiN and TiO2 as determined by quantitative reflection electron energy-loss spectroscopy. *Surf. Interface Anal.* **2002**, *33*, 230−237.

(3) Pendry, J. B. *Interaction of Atoms and Molecules with Solid Surfaces*; Springer, 1974; pp 201−211.

(4) Lindhard, J. On the Properties of a Gas of Charged Particles. *Dan. Mater. Fys. Medd.* **1954**, *28*, 1−57.

(5) Mermin, N. D. Lindhard Dielectric Function in the Relaxation-Time Approximation. *Phys. Rev. B* **1970**, *1*, 2362.

(6) Powell, C. J.; Swan, J. B. Origin of the characteristic electron energy losses in aluminum. *Phys. Rev.* **1959**, *115*, 869−875.

(7) Penn, D. R. Electron mean-free-path calculations using a model dielectric function. *Phys. Rev. B* **1987**, *35*, 482−486.

(8) Chantler, C. T.; Bourke, J. D. X-ray spectroscopic measurement of photoelectron inelastic mean free paths in molybdenum. *J. Phys. Chem. Lett.* **2010**, *1*, 2422−2427.

(9) Bourke, J. D.; Chantler, C. T. Measurements of Electron Inelastic Mean Free Paths in Materials. *Phys. Rev. Lett.* **2010**, *104*, No. 206601.

(10) Bourke, J. D.; Chantler, C. T. Electron Energy Loss Spectra and Overestimation of Inelastic Mean Free Paths in Many-Pole Models. *J. Phys. Chem. A* **2012**, *116*, 3202−3205.

(11) Chantler, C. T.; Nguyen, T. V. B.; Lowe, J. A.; Grant, I. P. Convergence of the Breit interaction in self-consistent and configuration-interaction approaches. *Phys. Rev. A* **2014**, *90*, No. 062504.

(12) Bourke, J. D.; Chantler, C. T. Momentum-dependent lifetime broadening of electron energy loss spectra: A self-consistent coupled-plasmon model. *J. Phys. Chem. Letts* **2015**, *6*, 314−319.

(13) Tanuma, S.; Powell, C. J.; Penn, D. R. Calculations of electorn inelastic mean free paths. II. Data for 27 elements over the 50−2000 eV range. *Surf. Interface Anal.* **1991**, *17*, 911−926.

(14) Seah, M. An accurate and simple universal curve for the energy-dependent electron inelastic mean free path. *Surf. Interface Anal.* **2012**, *44*, 497−503.

(15) Ridzel, O. Y.; Astašauskas, V.; Werner, W. S. Low energy (1−100 eV) electron inelastic mean free path (IMFP) values determined from analysis of secondary electron yields (SEY) in the incident energy range of 0.1−10 keV. *J. Electron Spectrosc. Relat. Phenom.* **2020**, *241*, 146824.

(16) Brown, A. M.; Sundararaman, R.; Narang, P.; Goddard, W. A., III; Atwater, H. A. Nonradiative plasmon decay and hot carrier dynamics: effects of phonons, surfaces, and geometry. *ACS Nano* **2016**, *10*, 957−966.

(17) Tanuma, S.; Shiratori, T.; Kimura, T.; Goto, K.; Ichimura, S.; Powell, C. J. Experimental determination of electron inelastic mean free paths in 13 elemental solids in the 50 to 5000 eV energy range by elastic-peak electron spectroscopy. *Surf. Interface Anal.* **2005**, *37*, 833−845.

(18) Hagemann, H.-J.; Gudat, W.; Kunz, C. Optical constants from the far infrared to the x-ray region: Mg, Al, Cu, Ag, Au, Bi, C, and Al 2 O 3. *JOSA* **1975**, *65*, 742−744.

(19) Palik, E. D. *Handbook of optical constants of solids*; Academic press, **1998**; Vol. 3.

(20) Chantler, C. T.; Bourke, J. D. Low-energy electron properties: Electron inelastic mean free path, energy loss function and the dielectric function. Recent measurements, applications, and the plasmon-coupling theory. *Ultramicroscopy* **2019**, *201*, 38−48.

(21) Chantler, C. T.; Bourke, J. D. In *International Tables for Crystallography, Vol. I*; Chantler, C. T.; Bunker, B. A.; Boscherini, F., Eds.; Wiley, 2024; pp 230−269.

(22) Rehr, J.; Albers, R.; Natoli, C.; Stern, E. New high-energy approximation for x-ray-absorption near-edge structure. *Phys. Rev. B* **1986**, *34*, 4350.

(23) Rehr, J. J.; Albers, R. C. Theoretical approaches to x-ray absorption fine structure. *Reviews of modern physics* **2000**, *72*, 621.

(24) Rehr, J. J.; Kas, J. J.; Vila, F. D.; Prange, M. P.; Jorissen, K. Parameter-free calculations of X-ray spectra with FEFF9. *Phys. Chem. Chem. Phys.* **2010**, *12*, 5503−5513.

(25) Newville, M. G. *Local thermodynamic measurements of dilute binary alloys using XAFS*. Ph.D. thesis, University of Washington, 1995.

(26) Newville, M. International X-ray Absorption Society. https://xaslib.xrayabsorption.org/spectrum//91/rawxafs (accessed: August 25, 2025).

(27) Chantler, C. T.; Tran, C. Q.; Paterson, D.; Cookson, D.; Barnea, Z. X-ray extended-range technique for precision measurement of the X-ray mass attenuation coefficient and Im (f) for copper using synchrotron radiation. *Phys. Lett. A* **2001**, *286*, 338−346.

(28) Chantler, C. T.; Tran, C. Q.; Barnea, Z.; Paterson, D.; Cookson, D. J.; Balaic, D. X. Measurement of the x-ray mass attenuation coefficient of copper using 8.85−20 keV synchrotron radiation. *Phys. Rev. A* **2001**, *64*, No. 062506.

(29) Glover, J. L.; Chantler, C. T.; Barnea, Z.; Rae, N. A.; Tran, C. Q.; Creagh, D. C.; Paterson, D.; Dhal, B. B. Measurements of the x-ray

mass-attenuation coefficient and imaginary component of the form factor of copper. *Phys. Rev. A* **2008**, *78*, No. 052902.
(30) Newville, M.; Ravel, B. *International Tables for Crystallography, Vol. I*; John Wiley & Sons, Ltd, 2024; pp 791−795.
(31) Bourke, J. D.; Chantler, C. T.; Joly, Y. FDMX: Extended X-ray Absorption Fine Structure Calculations Using the Finite Difference Method. *Journal of Synchrotron Radiation* **2016**, *23*, 551−559.
(32) Joly, Y.; Cabaret, D.; Renevier, H.; Natoli, C. R. Electron Population Analysis by Full-Potential X-Ray Absorption Simulations. *Phys. Rev. Lett.* **1999**, *82*, 2398.
(33) Joly, Y. X-ray absorption near-edge structure calculations beyond the muffin-tin approximation. *Phys. Rev. B* **2001**, *63*, No. 125120.
(34) Schalken, M. J.; Chantler, C. T. Propagation of uncertainty in experiment: structures of Ni (II) coordination complexes. *Journal of Synchrotron Radiation* **2018**, *25*, 920−934.
(35) Campbell, L.; Hedin, L.; Rehr, J.; Bardyszewski, W. Interference between extrinsic and intrinsic losses in x-ray absorption fine structure. *Phys. Rev. B* **2002**, *65*, No. 064107.
(36) Kas, J.; Sorini, A.; Prange, M.; Cambell, L.; Soininen, J. A.; Rehr, J. Many-pole model of inelastic losses in x-ray absorption spectra. *Phys. Rev. B* **2007**, *76*, No. 195116.
(37) Sayers, D. E.; Stern, E. A.; Lytle, F. W. New technique for investigating noncrystalline structures: Fourier analysis of the extended x-ray—absorption fine structure. *Physical review letters* **1971**, *27*, 1204.
(38) Gries, W. H. A universal predictive equation for the inelastic mean free pathlengths of X-ray photoelectrons and auger electrons. *Surf. Interface Anal.* **1996**, *24*, 38−50.
(39) Seah, M. P.; Dench, W. A. Quantitative electron spectroscopy of surfaces: A standard data base for electron inelastic mean free paths in solids. *Surf. Interface Anal.* **1979**, *1*, 2−11.
(40) Quinn, J. J. Range of excited electrons in metals. *Phys. Rev.* **1962**, *126*, 1453.
(41) Sze, S.; Moll, J.; Sugano, T. Range-energy relation of hot electrons in gold. *Solid-state electronics* **1964**, *7*, 509−523.
(42) Jablonski, A.; Powell, C. J. Relationships between electron inelastic mean free paths, effective attenuation lengths, and mean escape depths. *J. Electron Spectrosc. Relat. Phenom.* **1999**, *100*, 137−160.
(43) Powell, C. J.; Jablonski, A. Effective attenuation lengths for quantitative surface analysis by Auger-electron spectroscopy and X-ray photoelectron spectroscopy. *J. Electron Spectrosc. Relat. Phenom.* **2017**, *218*, 1−12.
(44) Powell, C. J. Attenuation lengths of low-energy electrons in solids. *Surf. Sci.* **1974**, *44*, 29−46.
(45) Kroeger, F. R.; Swenson, C. A. Absolute linear thermal expansion measurements on copper and aluminum from 5 to 320 K. *J. Appl. Phys.* **1977**, *48*, 853−864.
(46) Touloukian, Y. *Thermal Expansion: Metallic Elements and Alloys*; TPRC data series; Springer: USA, 1975.
(47) Wyckoff, R. *Crystal Structures*; Crystal Structures, Vol. *1*; Interscience Publishers, 1963.
(48) Kwei, C.; Chen, Y.-F.; Tung, C.; Wang, J. Electron inelastic mean free paths for plasmon excitations and interband transitions. *Surface science* **1993**, *293*, 202−210.
(49) Ashley, J. Energy loss rate and inelastic mean free path of low-energy electrons and positrons in condensed matter. *J. Electron Spectrosc. Relat. Phenom.* **1990**, *50*, 323−334.
(50) Chantler, C.; Bourke, J. Electron inelastic mean free path theory and density functional theory resolving discrepancies for low-energy electrons in copper. *J. Phys. Chem. A* **2014**, *118*, 909−914.
(51) Powell, C. J.; Jablonski, A. Evaluation of calculated and measured electron inelastic mean free paths near solid surfaces. *J. Phys. Chem. Ref. Data* **1999**, *28*, 19−62.
(52) Ding, Z.; Shimizu, R. A Monte Carlo modeling of electron interaction with solids including cascade secondary electron production. *Scanning: The Journal of Scanning Microscopies* **1996**, *18*, 92−113.
(53) Chantler, C. T.; Bourke, J. D. Significance, and tables of key physico-chemical parameters. In *International Tables for Crystallography, Vol. I*; Chantler, C. T.; Bunker, B. A.; Boscherini, F., Eds.; Dordrecht: Kluwer Academic Publishers, 2024; Chapter 2.25, pp 230−269.
(54) Dolinski, W.; Mroz, S.; Palczynski, J.; Gruzza, B.; Bondot, P.; Porte, A. Determination of Inelastic Mean Free Path of Electrons in Noble Metals. *Acta Phys. Polym., A* **1992**, *81*, 193−199.
(55) Shinotsuka, H.; Tanuma, S.; Powell, C. J.; Penn, D. R. Calculations of electron inelastic mean free paths. X. Data for 41 elemental solids over the 50 eV to 200 keV range with the relativistic full Penn algorithm. *Surf. Interface Anal.* **2015**, *47*, 871−888.
(56) Lindhard, J. On the properties of a gas of charged particles. *Kgl. Danske Videnskab. Selskab Mater.-Fys. Medd.* **1954**, *28*, 1−57.
(57) Krause, M. O.; Oliver, J. Natural widths of atomic K and L levels, K α X-ray lines and several KLL Auger lines. *J. Phys. Chem. Ref. Data* **1979**, *8*, 329−338.
(58) Campbell, J.; Papp, T. Widths of the atomic K−N7 levels. *Atomic Data and Nuclear Data Tables* **2001**, *77*, 1−56.
(59) Beni, G.; Platzmann, P. M. Temperature and polarization dependence of extended x-ray absorption fine-structure spectra. *Phys. Rev. B* **1976**, *14*, 1514.
(60) Greegor, R. B.; Lytle, F. W. Extended x-ray absorption fine structure determination of thermal disorder in Cu: Comparison of theory and experiment. *Phys. Rev. B* **1979**, *20*, 4902−4907.
(61) Bearden, J. A. X-ray wavelengths. *Rev. Mod. Phys.* **1967**, *39*, 78−124.
(62) Kraft, S.; Stümpel, J.; Becker, P.; Kuetgens, U. High resolution x-ray absorption spectroscopy with absolute energy Calibration for the determination of absorption edge energies. *Rev. Sci. Instrum.* **1996**, *67*, 681−687.

https://doi.org/10.1021/acs.jpca.6c00232
J. Phys. Chem. A 2026, 130, 1940−1947